Polymer 50 (2009) 5326–5332

Contents lists available at ScienceDirect

Polymer

journal homepage: www.elsevier.com/locate/polymer

Electrophoretical stretching of DNA in a hybrid microchannel

Zuo Chuncheng [1], Ji Feng*, Cao Qianqian [1]

College of Mechanical Science and Engineering, Jilin University, Changchun 130025, China

ARTICLE INFO

Article history:
Received 14 February 2009
Received in revised form
15 September 2009
Accepted 15 September 2009
Available online 22 September 2009

Keywords:
DNA
Hybrid microchannel
Brownian dynamics

ABSTRACT

The electrophoretical stretching of DNA in a hybrid microchannel is analyzed in this paper. The channel comprises a large insulating cylinder and a hyperbolic contraction that can cause the DNA deformation. Brownian dynamics simulation is used to characterize the dynamical stretching process of a long T4 DNA in hybrid microchannels. The computational results show us the larger average extension of DNA in cylinder-hybridized microchannels than that in the single microcontractions due to the prestretched effect of cylinder on DNA. Moreover, the location and the radius of the insulating cylinder in hybrid microchannels have great effects on the stretching behavior of DNA.

1. Introduction

Understanding the dynamics of DNA stretching is of great importance in molecular biology and genetics. The DNA molecules appeared to be of random coiled conformation in a solution, which has made the gene mapping more complicated and time consuming. Thus it is necessary for genomic analysis to stretch DNA. Many techniques, such as extending DNA with tweezers [1–3], surface [4–8], nanofluidic confinement [9–11], uniform flows [12] and electric field [13], as well as in velocity gradients [14–27] and electric field gradients [28–32], have been developed during the past decade. These studies have showed great progress in design of microchannels capable of manipulating DNA transportation and extension for gene mapping.

Among these techniques, variation in the initial state of polymer can result in the molecular individualism, where some molecules may strongly deform while other molecules may weakly extend. To solve this question, the prestretched conformation caused by shearing before elongational flow can be used to increase the extension of polymer [33]. Preconditioning arising from obstacle array located before a contraction has also expected to control the stretching process of polymers [34]. Unfortunately, the dependence of prestretched effects on the size of the hybrid structure may obtain little consideration.

The purpose of this paper is to analyze the preconditioning by a large cylinder before a microcontraction. We investigate the influences of size and location of cylinder on the preconditioning. The radius of cylinder is larger than the least contraction, which is different from the conditions in the Ref. [34] where the size of the obstacle is not only smaller than the contraction but also much smaller than the width of inlet. High stretching efficiency of DNA can be achieved in this hybrid microchannel. Brownian dynamics is used to simulate the stretching behavior of T4 DNA. The geometry of this hybrid microchannel is presented in Section 2, followed in Section 3 by systematic models and governing equations. Results and discussions are presented in Section 4, with conclusions given in Section 5.

2. A hybrid microchannel

A schematic diagram of the hybrid microchannel is shown in Fig. 1. It can be seen, from Fig. 1, that the hybrid microchannel consists of a large insulating cylinder and a hyperbolic contraction modeled by equation $y = c/(x + 2c/h_1)$. The widths of inlet, hyperbolic contraction and outlet are $h_1 = 200\ \mu m$, $h_2 = 3.8\ \mu m$, $h_3 = 200\ \mu m$, respectively. The lengths of inlet, transition region, hyperbolic contraction and outlet are $l_1 = 1.5$ mm, $l_c = 80\ \mu m$, $l_2 = 1.52$ mm, $l_3 = 1.5$ mm, respectively. The hyperbolic parameter is $c = 155\ \mu m^2$. The width of cylindrical obstruction is $h_r = 100\ \mu m$. The distance of cylinder to the grid origin l_r can be varied from

* Corresponding author. Tel.: +86 13019229680; fax: +86 43185095288.
E-mail addresses: zuocc@jlu.edu.cn (Z. Chuncheng), jifeng0203@hotmail.com (J. Feng), caoqianqian@email.jlu.edu.cn (C. Qianqian).
[1] Tel.: +86 13019229680; fax: +86 43185095288.

0032-3861/$ – see front matter © 2009 Elsevier Ltd. All rights reserved.
doi:10.1016/j.polymer.2009.09.043

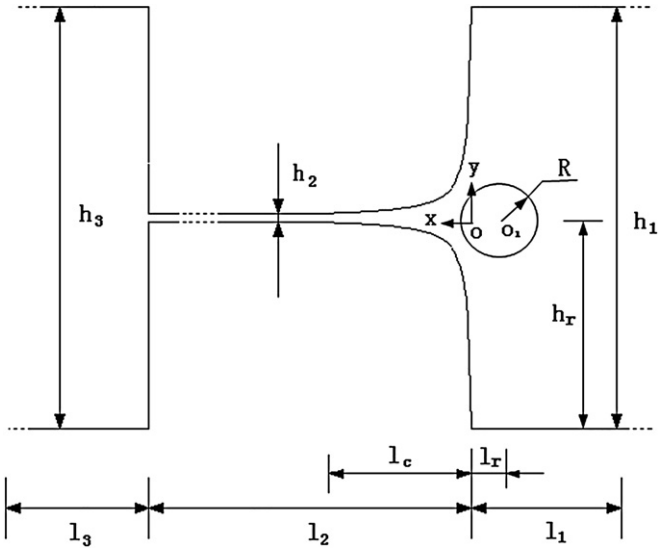

Fig. 1. A schematic diagram of the hybrid microchannel, which consists of a large insulating cylinder and a hyperbolic contraction. The hyperbolic equation can be expressed as: $y = c/(x + 2c/h_1)$. Here, $c = 155\ \mu m^2$.

10 μm to 50 μm in this paper. And the radius of cylinder R can be changed from 10 μm to 30 μm.

When an electric field is applied to the both ends of the hybrid microfluidic channels, the T4 DNA molecules can be forced into inlet in the right side, through a cylindrical barrier and then a hyperbolic contraction, and out of the microgeometries in the left side. Due to the gradients of electric field in the regions of cylinder and hyperbolic contraction, the long DNA molecules can be stretched easily.

3. Systematic models

T4 DNA is modeled as N beads connected by $N_s = N-1$ entropic springs. Brownian dynamics simulation with hydrodynamic interactions is first introduced by Ermak and McCammon [35]. The velocity for bead i is

$$\frac{dr_i}{dt} = \mu E(r_i) + \sum_{j=1}^{N} \frac{\partial D_{ij}}{\partial r_j} + \sum_{j=1}^{N} \frac{D_{ij} \cdot \left(F_j^{es} + F_j^{ev} + F_j^{wall}\right)}{k_B T} + \left(\frac{6}{\Delta t}\right)^{1/2} \sum_{j=1}^{i} B_{ij} \cdot n_j \quad (1)$$

where μ is the mobility of DNA, $\mathbf{r}_i$ the coordinate vector of bead i, $\mathbf{E}$ the electric field, $\mathbf{D}_{ij}$ the mobility tensor, $\mathbf{F}_j^{es}$ the effective spring force, $\mathbf{F}_j^{ev}$ the excluded volume force to prevent unrealistic crossings and collisions between beads, $\mathbf{F}_j^{wall}$ the repulsion force caused by the hyperbolic contraction walls, k_B the Boltzmann constant, T the absolute temperature, Δt the time step, $\mathbf{B}_{ij}$ the coefficient tensor, and $\boldsymbol{n}_j$ is a random vector uniformly distributed in each of the three directions over the interval $[-1, 1]$.

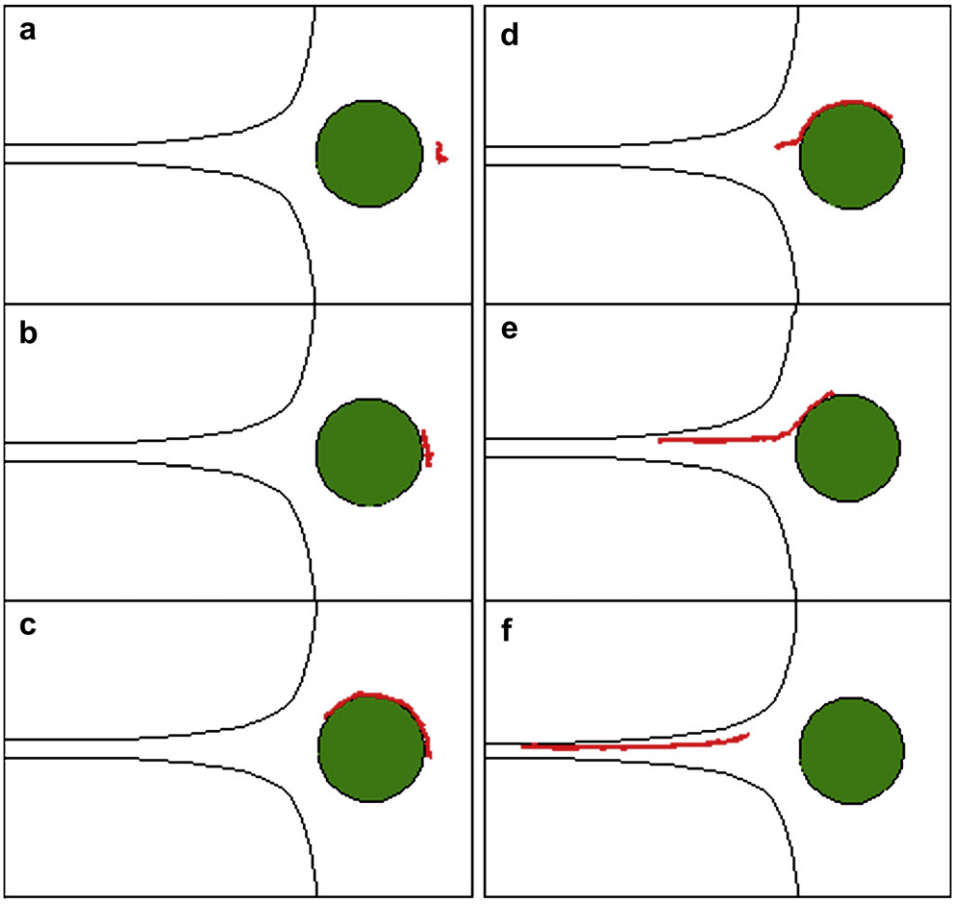

Fig. 2. Images of long T4 DNA molecule in a hybrid microchannel at De = 23, where the radius of cylinder is $R = 15\ \mu m$ and the center of the cylinder is located at $O_1(-13\ \mu m, 100\ \mu m)$.

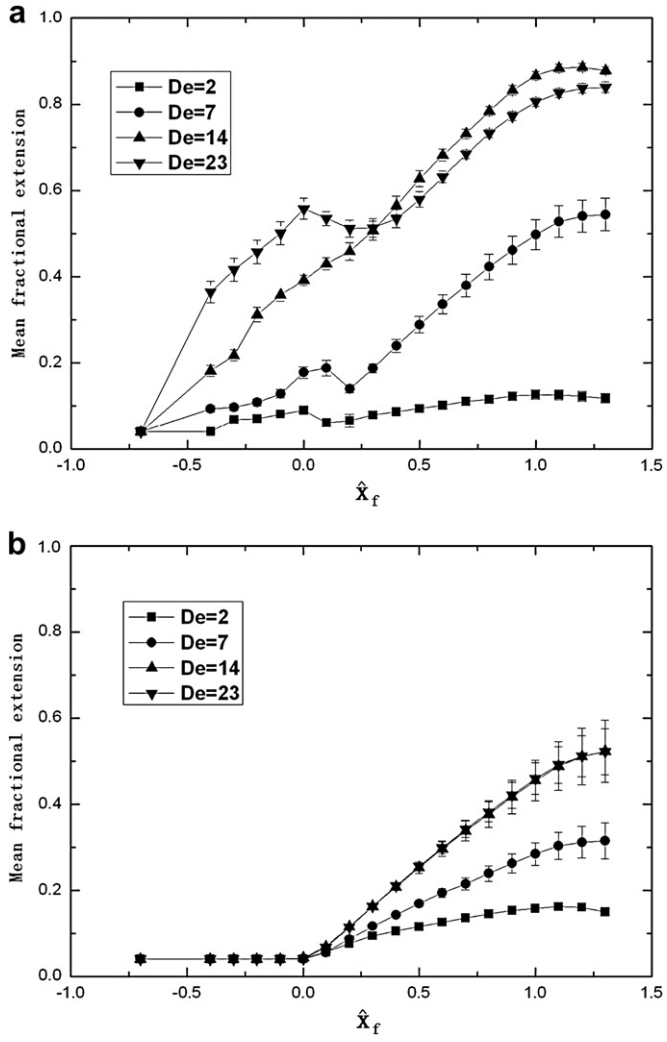

Fig. 3. Plots of mean fractional extension against the x-coordinate of the front of the DNA $\hat{x}_f = x_f/l_c$ both in a hybrid microchannel (a) and in a single hyperbolic contraction (b).

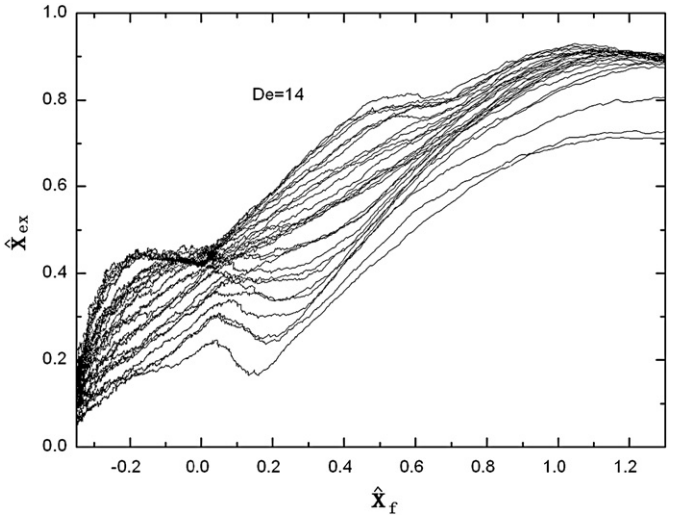

Fig. 4. Plots of 30 individual fractional extensions $\hat{x}_{ex} = x_{ex}/L$ as a function of $\hat{x}_f = x_f/l_c$ in a hybrid microchannel, where the radius of cylinder is $R = 15$ μm and the center of the cylinder is located at $O_1(-13\ \mu m, 100\ \mu m)$.

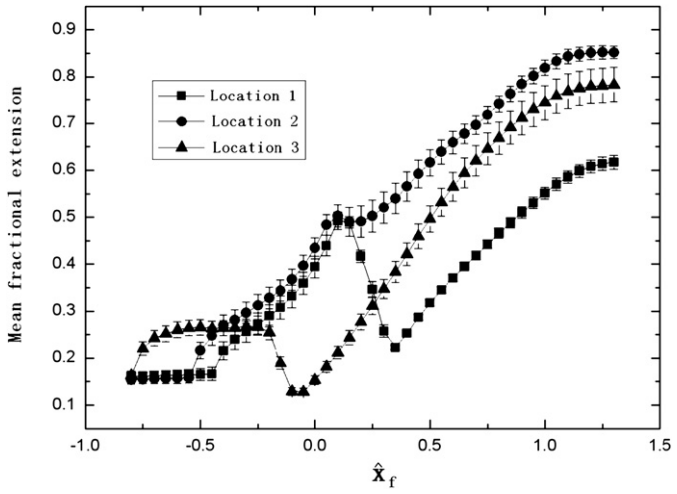

Fig. 5. Plots of mean fractional extension against the x-coordinate of the front of the DNA $\hat{x}_f = x_f/l_c$ in the hybrid microchannels with $R = 25$ μm at De = 14: $O_1(-13\ \mu m, 100\ \mu m)$ (square data); $O_1(-20\ \mu m, 100\ \mu m)$ (cycle data); $O_1(-40\ \mu m, 100\ \mu m)$ (triangle data).

Hydrodynamic interaction is introduced into the stochastic differential equations through the mobility tensor $\mathbf{D}_{ij}$. In our model, the Rotne-Prager tensor is used [36].

$$D_{ij} = \frac{k_B T}{6\pi\eta a} I_{3*3} \quad \text{if } i = j \tag{2}$$

$$D_{ij} = \frac{k_B T}{8\pi\eta r_{ij}}\left[\left(I_{3*3} + \frac{r_{ij}r_{ij}}{r_{ij}^2}\right) + \frac{2a^2}{r_{ij}^2}\left(\frac{1}{3}I_{3*3} - \frac{r_{ij}r_{ij}}{r_{ij}^2}\right)\right] \quad \text{if } i \neq j \text{ and } r_{ij} > 2a \tag{3}$$

$$D_{ij} = \frac{k_B T}{6\pi\eta a}\left[\left(1 - \frac{9}{32}\frac{r_{ij}}{a}\right)I_{3*3} + \frac{3}{32}\frac{r_{ij}r_{ij}}{a r_{ij}}\right] \quad \text{if } i \neq j \text{ and } r_{ij} \leq 2a \tag{4}$$

where η is the solvent viscosity, a the radius of the beads, $\mathbf{r}_{ij} = \mathbf{r}_i - \mathbf{r}_j$, $r_{ij} = \|r_{ij}\|$, and $\mathbf{I}_{3*3}$ is the identity tensor.

In addition, the coefficient tensor $\mathbf{B}_{ij}$ is related to the mobility tensor $\mathbf{D}_{ij}$ by:

$$D_{ij} = \sum_{l=1}^{N} B_{il} \cdot B_{jl} \tag{5}$$

The effective spring force, $\mathbf{F}_j^{es}$, is given by

$$F_j^{es} = \begin{cases} F_1^s & \text{if } j = 1 \\ F_j^s - F_{j-1}^s & \text{if } 1 < j < N \\ F_{N-1}^s & \text{if } j = N \end{cases} \tag{6}$$

where $\mathbf{F}_j^s$ is the spring force associated with spring j. In our model, the Pade approximation is used to model the inverse Langevin force law [37]:

$$F_j^s = \frac{k_B T}{b_K}\frac{Q_j}{Q_0}\left[\frac{3 - (Q/Q_0)^2}{1 - (Q/Q_0)^2}\right] \tag{7}$$

where $\mathbf{Q}_j = \mathbf{r}_{j+1} - \mathbf{r}_j$ is the spring connector vector for spring j, Q the magnitude of $\mathbf{Q}_j$, Q_0 the maximum extensibility of each spring, and b_K is the Kuhn length which is twice the persistence length l^p, i.e. $b_K = 2l^p$.

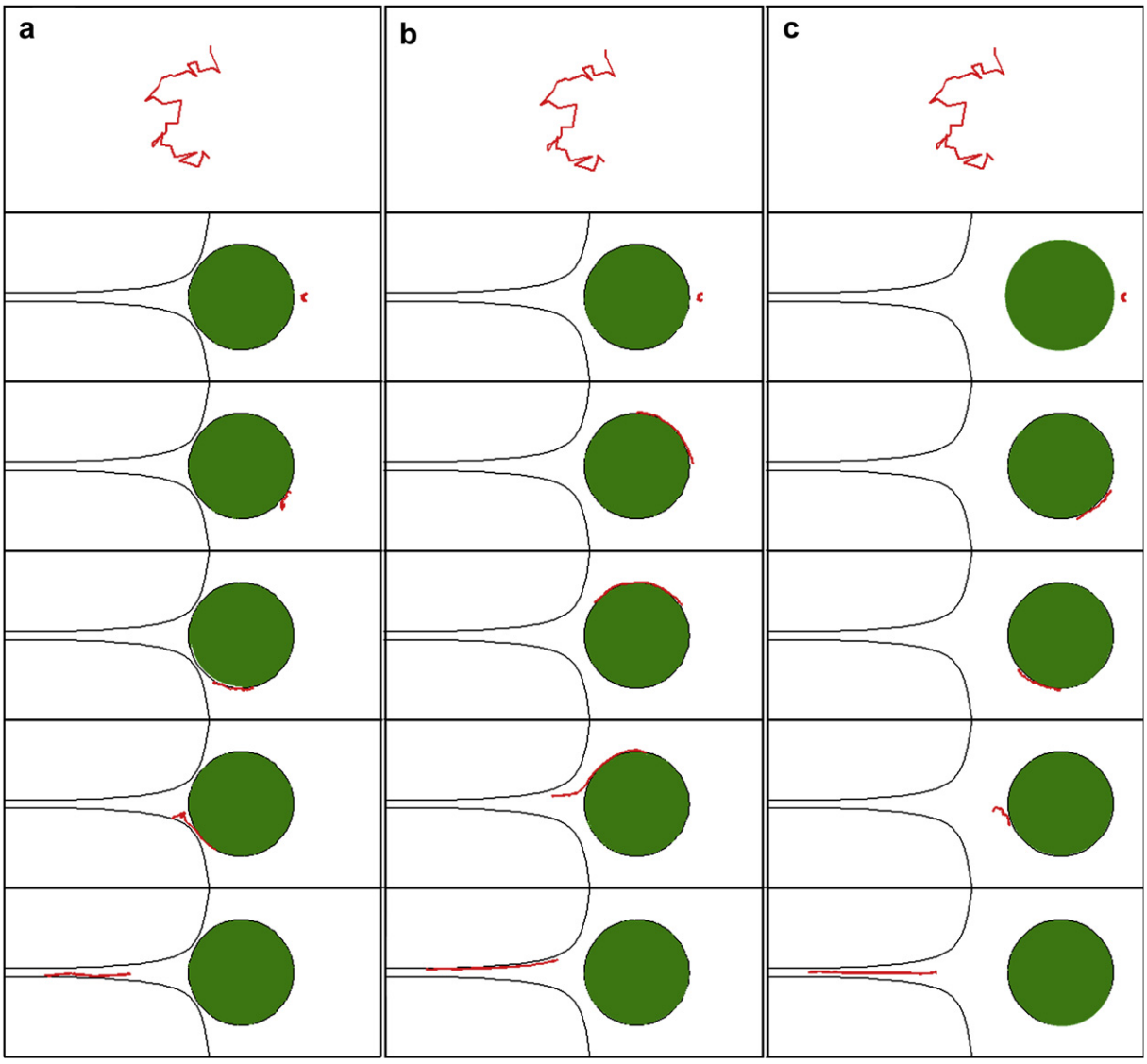

Fig. 6. Images of long T4 DNA molecule in the hybrid microchannels at De = 14, (a) $R = 15$ μm, $O_1(-13$ μm, 100 μm); (b) $R = 15$ μm, $O_1(-20$ μm, 100 μm); (c) $R = 15$ μm, $O_1(-40$ μm, 100 μm).

Excluded volume interactions are incorporated into our model to capture good solvents of DNA in aqueous solution. In the form of Gaussian coils, the excluded volume potential between two beads of the chain can be expressed as [27,38,39]:

$$U_{ij}^{\mathrm{ev}} = \frac{1}{2}\nu k_{\mathrm{B}}TN_{\mathrm{k,s}}^2\left(\frac{3}{4\pi S_{\mathrm{s}}^2}\right)^{3/2}\exp\left[\frac{-3r_{ij}^2}{4S_{\mathrm{s}}^2}\right] \tag{8}$$

where ν is the excluded volume parameter, $N_{\mathrm{k,s}}$ the number of Kuhn segments per spring, and $S_{\mathrm{s}} = \sqrt{(N_{\mathrm{k,s}}b_K^2)/6}$ is the radius of gyration of each submolecule.

To realize the physical confinement of hyperbolic contraction walls, a bead-wall repulsive potential is introduced [26]:

$$U_j^{\mathrm{wall}} = \begin{cases} \frac{A_{\mathrm{wall}}}{3b_K\delta_{\mathrm{wall}}^2}(h-\delta_{\mathrm{wall}})^3 & \text{if } h < \delta_{\mathrm{wall}} \\ 0 & \text{if } h > \delta_{\mathrm{wall}} \end{cases} \tag{9}$$

where h is the distance of bead j from the wall in the wall-normal direction, δ_{wall} the cut-off distance, and A_{wall} is the repulsive energy constant. In our model, we use $A_{\mathrm{wall}} = 25k_{\mathrm{B}}T$ and $\delta_{\mathrm{wall}} = b_K N_{\mathrm{k,s}}^{1/2}/2$.

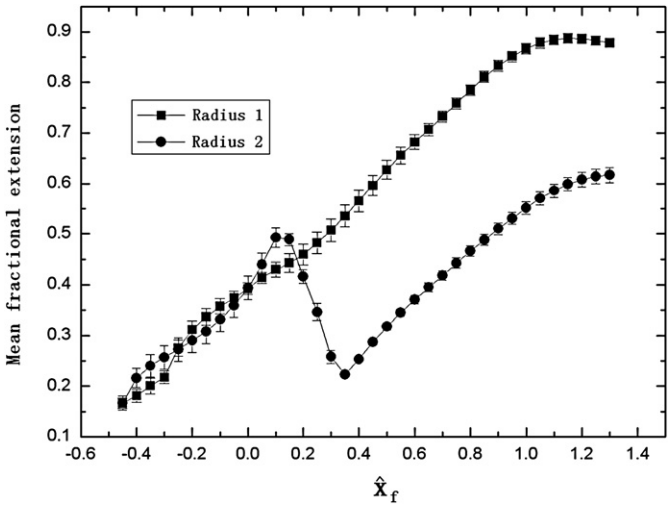

Fig. 7. Plots of mean fractional extension against the x-coordinate of the front of the DNA $\hat{x}_{\mathrm{f}} = x_{\mathrm{f}}/l_{\mathrm{c}}$ in the hybrid microchannels with $O_1(-13$ μm, 100 μm) at De = 14: $R = 15$ μm (square data); $R = 25$ μm (cycle data).

It should be noted that there is no attractive potential between the polymers and surface of cylinder or hyperbolic contraction, which is different from the method in the Ref. [7], where one of the ends of the polymer is tethered on the chemically modified surface.

Forces on bead j due to excluded volume effect and molecule-wall repulsion can be obtained from the usual relation, $F_j = -\nabla_j U$.

The three-step "predictor–corrector" method is used to be integration scheme, which promise higher accuracy and less simulation time. The details of algorithm can be found in Refs. [40,41].

T4 DNA molecule is modeled as a bead-spring chain of 35 beads connected by 34 springs, where the radius of each bead is $a = 77$ nm. The length of each spring corresponds to the product of the Kuhn length b_K and the number of Kuhn segments per spring

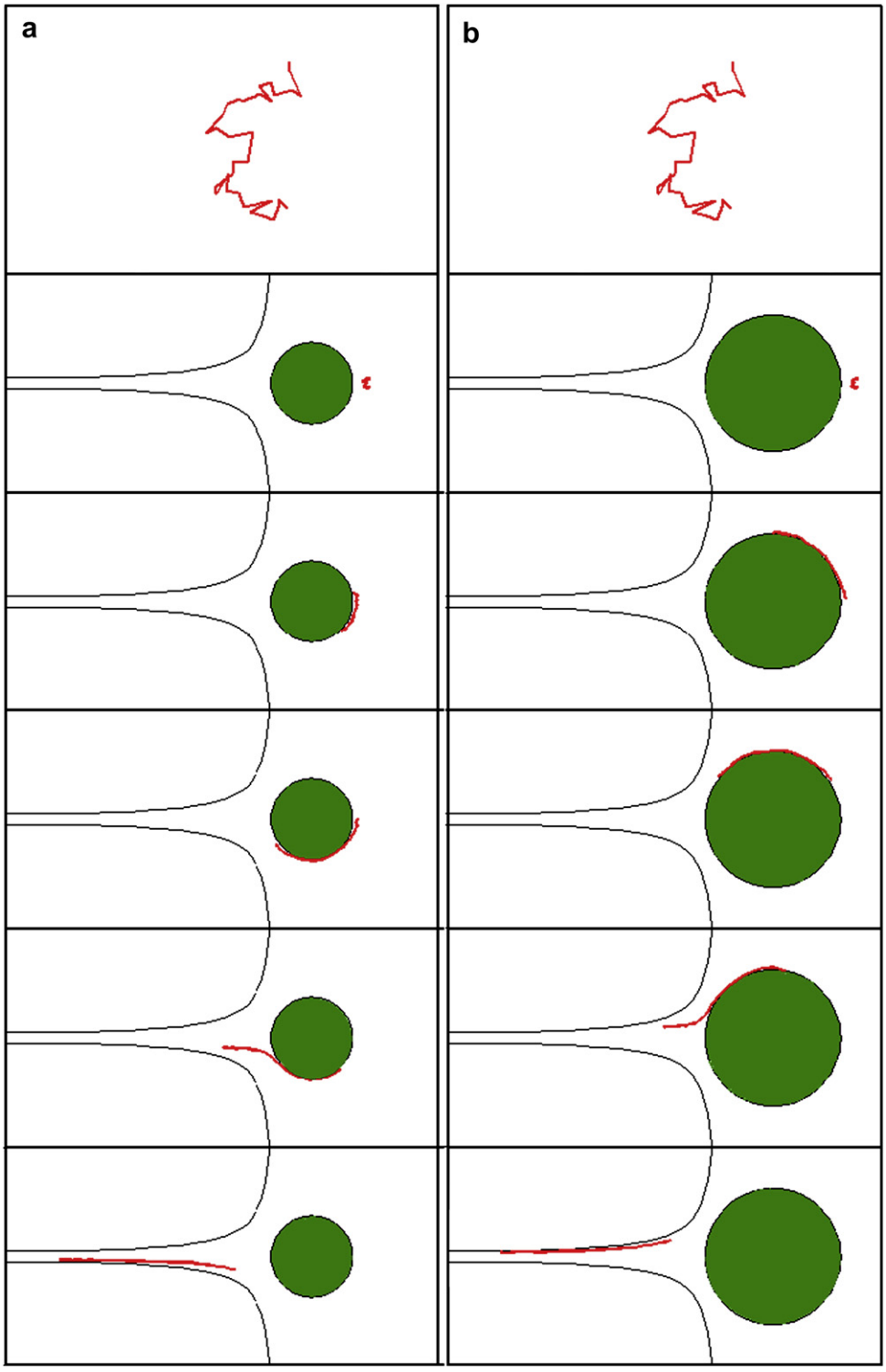

Fig. 8. Images of long T4 DNA molecule in the hybrid microchannels at De = 14, (a) $R = 15$ μm, $O_1(-13$ μm, 100 μm); (b) $R = 25$ μm, $O_1(-13$ μm, 100 μm).

$N_{k,s}$, where $b_K = 106$ nm and $N_{k,s} = 19.8$. The parameter of the excluded volume potential is set to be $\nu = 0.0012\ \mu m^3$.

Deborah number (De) is used to scale the longest relaxation time of DNA τ and the inverse of strain rate $1/\dot{\varepsilon}$: $De = \dot{\varepsilon}\tau = \mu E_2 \tau / l_c$, where μ is the measured electrophoretic mobility of the T4 DNA, and E_2 is the maximum electric field strength at the contraction exit. In this paper, the longest relaxation time is obtained to be 1.7 s.

4. Results and discussions

4.1. Stretching behavior of DNA in a hybrid microchannel

Fig. 2 shows the stretching behavior of long T4 DNA molecule in a hybrid microchannel at De = 23, where the radius of cylinder is $R = 15\ \mu m$ and the center of the cylinder is located at $O_1(-13\ \mu m, 100\ \mu m)$. T4 DNA electrophoretically passes through the cylindrical obstruction from the right side to the left side, and then moves to the hyperbolic contraction. It can be seen, from Fig. 2, that DNA molecule begins to stretch in the *y*-direction, when it reaches the front surface of cylinder. In other words, the coiled conformation of T4 DNA in a solution has changed to be the stretched state. Due to the location of the backside of cylinder at the entrance of the hyperbolic contraction, DNA electrophoretically moves to the back of the cylindrical obstruction and at the same time enter the hyperbolic geometry in a hybrid microchannel. T4 DNA has large extension in the hyperbolic contraction shown in Fig. 2(f), where the strain rate is above the stretching critical value (De = 0.5).

The comparison of mean factional extension of DNA in a hybrid microchannel and that in a single hyperbolic contraction against the *x*-coordinate of the front of the DNA $\widehat{x}_f = x_f/l_c$ at De = 2, 7, 14 and 23 is shown in Fig. 3. When De changes from the lower case (De = 2) to the intermediate case (De = 14), the extension of DNA obviously increases due to strong electric field gradients in microchannels [42]. Moreover, the deformation of DNA in the hybrid microchannel is obviously stronger due to its preconditioning effect than that in the single microchannel. It also should be noted that the stretching rate seems to reach a plateau, where the average mean fractional extension does not clime up any more with the variation of De from 14 to 23.

Fig. 4 shows the individualistic stretching behavior of DNA in a hybrid microchannel, where $O_1(-13\ \mu m, 100\ \mu m)$ and $R = 15\ \mu m$. Some curves show rapid extensions and other curves show slow extensions. The diversity of extension process is sensitive to the initial conformation of DNA, but the preconditioning effect can to some extent reduce this sensitivity.

4.2. Effects of location and size of cylindrical obstruction

We have found that the geometry of the hybrid microchannel has great effect on the stretching dynamics of DNA. In order to illustrate this effect, we consider the mean fractional extension of DNA in three hybrid microgeometries with the radius of cylindrical obstruction 25 μm at De = 14 as shown in Fig. 5. The variety in final mean fractional extension stems from the differences of stretching process of DNA. The black square in Fig. 5 represents the mean fractional extension of DNA in the hybrid microchannel, where the center of the cylinder is $O_1(-13\ \mu m, 100\ \mu m)$. In this case, DNA molecules experience the stretch-compress-stretch process. The great compression of DNA at the back of the cylinder results in the smallest final extension. The black cycle in Fig. 5 corresponds to mean fractional extension of DNA in the hybrid microchannel with the center of the cylinder $O_1(-20\ \mu m, 100\ \mu m)$, where almost two consecutive stretching processes can be found. The little compression of DNA at the transition region from the backside of cylinder to the hyperbolic contraction leads to the largest extension. The black triangles are data for DNA molecules in the hybrid channel, where the center of the cylindrical is $O_1(-40\ \mu m, 100\ \mu m)$. With the same initial conformation, the comparison of stretching dynamics of DNA in three hybrid microchannels is also shown in Fig. 6.

To assess the effect of the size of cylinder on the stretching behavior of DNA, the cases with the radius of cylinder $R = 15\ \mu m$ and $R = 25\ \mu m$ can be straightforwardly compared. The computational results of mean fractional extension against the *x*-coordinate of the front of the DNA $\widehat{x}_f$ at De = 14 is presented in Fig. 7, where the center of cylinder is $O_1(-13\ \mu m, 100\ \mu m)$. It can be found, from Fig. 7, that the mean fractional extension in the case of $R = 25\ \mu m$ is smaller than that in case of $R = 15\ \mu m$ due to strong compression dynamics of DNA in the backside of obstruction. Fig. 8 shows the comparison of stretching dynamics of DNA in these two hybrid microgeometries. The difference in size of cylinder in the hybrid microchannel results in the variety in the stretching behavior and fractional extension.

5. Conclusion

This paper is an attempt to study the extension process and pre-deformation of polymer in a hybrid microchannel, which consists of a large insulating cylinder and a hyperbolic contraction. To verify the high performance of this microgeometry, we have used the bead-spring Brownian dynamics to simulate the stretching behavior of long T4 DNA in this hybrid microchannel and compared with that in the single hyperbolic contraction.

The computational results show that the mean fractional extension in the hybrid microchannel is much higher than that in the single hyperbolic microcontraction. More rapid and increasing extension of DNA in hybrid microgeometry can stem from the higher De value. At De = 14, the highest mean fractional extension in the hybrid microchannel can achieve about 0.9 without the use of a gel matrix. The location and size of the insulating cylinder have great effects on the stretching dynamics due to the pre-deformation of DNA through the cylinder. Moreover, the final extension of DNA in the hybrid microchannel is sensitive to the compression behavior of DNA at the back of cylindrical obstruction.

The new idea of the combination of two different geometries to increase the extension of DNA can help in designing the better stretching techniques for biopolymers and can be extended to other fields of microchannels.

Acknowledgements

This work is supported by the Chinese National Natural Science Foundation Grant No.10572053, the Doctor Foundation Grant No. 20040183057, and the Chinese National Programs for High Technology Research and Development Grant No. 2006AA04Z305.

References

[1] Smith SB, Cui Y, Bustamante C. Science 1996;271:795–9.
[2] Simmons RM, Finer JT, Chu S, Spudich JA. Biophys J 1996;70:1813–22.
[3] Amblard F, Yurke B, Pargellis A, Leibler S. Rev Sci Instrum 1996;67:818–27.
[4] Schwartz DC, Li X, Hernandez LI, Ramnarain SP, Huff EJ, Wang YK. Science 1993;262:110–4.
[5] Petit CAP, Carbeck JD. Nano Lett 2003;3:1141–6.
[6] Michalet X, Ekong R, Fougerousse F, Rousseaux S, Schurra C, Hornigold N, et al. Science 1997;277:1518–23.
[7] Dimalanta ET, Lim A, Runnheim R, Lamers C, Churas C, Forrest DK, et al. Anal Chem 2004;76:5293–301.
[8] Aston C, Hiort C, Schwartz DC. Methods Enzymol 1999;303:55–73.
[9] Tegenfeldt JO, Prinz C, Cao H, Chou S, Reisner WW, Riehn R, et al. Proc Natl Acad Sci U S A 2004;101:10979–83.
[10] Li W, Tegenfeldt JO, Chen L, Austin RH, Chou SY, Kohl P, et al. Nanotechnology 2003;14:578–83.
[11] Riehn R, Lu M, Wang Y-M, Lim SF, Cox EC, Austin RH. Proc Natl Acad Sci U S A 2005;102:10012–6.
[12] Perkins TT, Smith DE, Larson RG, Chu S. Science 1995;268:83–7.

[13] Ferree S, Blanch HW. Biophys J 2003;85:2539–46.
[14] Tegenfeldt JO, Bakajin O, Chou C-F, Chan SS, Austin R, Fann W, et al. Phys Rev Lett 2001;86:1378–81.
[15] Larson JW, Yantz GR, Zhong Q, Charnas R, D'Antoni CM, Gallo MV, et al. Lab Chip 2006;6:1187–99.
[16] Chan EY, Goncalves NM, Haeusler RA, Hatch AJ, Larson JW, Maletta AM, et al. Genome Res 2004;14:1137–46.
[17] Hofmann T, Winkler RG, Reineker P. Phys Rev E 2000;61:2840–7.
[18] Ripoll M, Winkler RG, Gompper G. Phys Rev Lett 2006;96:188302.
[19] Winkler RG. Phys Rev Lett 2006;97:128301.
[20] Petera D, Muthukumar M. J Chem Phys 1999;111:7614–23.
[21] Liu S, Ashok B, Muthukumar M. Polymer 2004;45:1383–9.
[22] Streek M, Schmid F, Duong TT, Anselmetti D, Ros A. Phys Rev E 2005;71:011905.
[23] Panwar AS, Kumar S. Macromolecules 2006;39:1279–89.
[24] Panwar AS, Kumar S. J Chem Phys 2003;118:925–36.
[25] Larson RG, Hu H, Smith DE, Chu S. J Rheol 1999;43:267–304.
[26] Jendrejack RM, Schwartz DC, Pablo JJd, Graham MD. J Chem Phys 2004;120:2513–29.
[27] Jendrejack RM, Pablo JJd, Graham MD. J Chem Phys 2002;116:7752–9.
[28] Randall GC, Doyle PS. Phys Rev Lett 2004;93:058102.
[29] Randall GC, Doyle PS. Macromolecules 2005;38:2410–8.
[30] Randall GC, Schultz KM, Doyle PS. Lab Chip 2006;6:516–25.
[31] Kim JM, Doyle PS. Lab Chip 2007;7:213–25.
[32] Kim JM, Doyle PS. J Chem Phys 2006;125:074906.
[33] Larson RG. J Non-Newton Fluid Mech 2000;94:37–45.
[34] Balducci A, Doyle PS. Macromolecules 2008;41:5485–92.
[35] Ermak DL, McCammon JA. J Chem Phys 1978;69:1352–60.
[36] Rotne J, Prager S. J Chem Phys 1969;50:4831–7.
[37] Cohen A. Rheol Acta 1991;30:270–3.
[38] Jendrejack RM, Schwartz DC, Graham MD, Pablo JJd. J Chem Phys 2003;119:1165–73.
[39] Schroeder CM, Shaqgeh ESG, Chu S. Macromolecules 2004;37:9242–56.
[40] Somasi M, Khomami B, Woo NJ, Hur JS, Shaqfeh ESG. J Non-Newton Fluid Mech 2002;108:227–55.
[41] Hsieh CC, Li L, Larson RG. J Non-Newton Fluid Mech 2003;113:147–91.
[42] Chuncheng Z, Feng J, Qianqian C, Jingsong Y. Polymer 2008;49:809–15.